Arc Simulation Model for Three-Phase Electro-Metallurgical Furnaces

G.A. Sævarsdottir, J.A. Bakken, V.G. Sevastyanenko, Liping Gu

Department of Materials Technology and Electrochemistry,
Norwegian University of Science and Technology, N-7491 Trondheim, Norway

gudrunsa @ matek.sintef.no, jabakken@chembio.ntnu.no, vicsev@usa.net, gulipin@hotmail.com

Keywords: Electric Arc, Furnace, Silicon, Ferrosilicon

ABSTRACT

A typical three-phase submerged-arc furnace for production of silicon metal and ferrosilicon has arc currents ~100 kA, phase voltages ~100 V and total furnace power ~10 – 60 MW. The arcs burn in gas filled cavities or "craters", where the main atomic components of the plasma mixture are *silicon, oxygen* and *carbon*. Two quite different simulation models for high-current AC arcs have been developed: the simple PC based *Channel Arc Model (CAM)*, and the more sophisticated *Magneto-Fluid-Dynamic (MFD)* model, which is here described in some detail. CAM simulation results have previously been reported at INFACON-8 [1].

The coupling between the arcs and the AC power source is described by a complete three-phase *Electric Circuit Model.*

Modelling results for ~1 kA laboratory AC arcs agree satisfactorily with electrical measurements. In the industrial ~100 kA case the simulations clearly show that the maximum possible arc length is 5 – 10 cm, which is much less than previously assumed.

Preliminary results with a *Cathode Sub-Model* for high-current AC arcs indicate that the cathode current density varies considerably during an AC period, while the spot radius remains almost constant. Model simulations further show that the influence of the easily ionizable contaminants *Ca* and *Al* on arc behaviour is much less than expected. Preliminary studies of the effect of *Fe* vapour on the plasma properties suggest that modelling results obtained for silicon metal are also applicable to ferrosilicon furnaces.

Arc splitting – i.e. several parallel arcs appearing simultaneously – may also play a role.

1. INTRODUCTION

The conventional production processes for silicon metal and ferrosilicon are based on the same principles as the original processes from before world war one. The raw materials for industrial production of silicon metal are quartz, coal and coke with addition of iron oxide in the case of ferrosilicon. These materials are mixed and charged continuously from the top into the cylindrical *three-phase* furnace, where they are warmed up as they descend slowly towards the hot inner zone around the three AC arcs. Prebaked *carbon* electrodes are used in silicon metal furnaces and *Søderberg* electrodes in ferrosilicon furnaces. In these furnaces – often referred to as *submerged-arc furnaces* - the arcs burn in gas filled cavities, called *craters*, formed underneath and around the lower part of the electrodes. Here most of the electric power is dissipated. A part of the electrode current is, however, conducted through the hot mixture of unreacted charge materials and silicon carbide in the crater walls surrounding the electrodes, thus *bypassing* the arcs. The arc spots are normally assumed to be situated on the electrode tips and on the metal pool surface, or the porous silicon carbide matrix that forms the crater bottom and is filled with metal. However, there is some evidence that the arc can burn from the side of the electrode. This can be seen both from electrode movements and from the morphology of the electrode tip.

The overall chemical reaction can be written

$$SiO_2(liq,sol) + 2C(sol) = Si(liq) + 2CO(gas).$$

Typical data for industrial silicon metal furnaces are: furnace diameter 5 - 8 m, electrode diameter 1 - 1.5 m, total furnace power 10-30 MW, electrode current 50-100 kA RMS. The phase voltages as measured between the electrodes and the furnace bottom are usually 100 V. The electrical energy consumption is 11-13 MWh/ton Si. The production rate is 1-2 ton Si/h. Ferrosilicon furnaces have even bigger dimensions, higher power 20 - 60 MW and electrode currents up to 150 kA RMS.

The arcs are typically less than 10 cm long with a conducting core diameter of 5 - 10 cm. In this work one is obviously dealing with relatively short high-power electric arcs. The ambient atmosphere consists of *SiO* and *CO* gas plus small amounts of metal vapours (mainly *Si* and *Fe* with *Ca* and *Al* as contaminants). The ambient pressure is slightly above 1 bar. Arc temperatures are in the usual range 10,000-30,000 K. The crater wall and bottom temperatures are around 2,000 K.

Due to the large dimensions and thermally and chemically hostile environment in the craters, it is very difficult to observe directly the processes taking place in the inner zones of the furnace. The available access for advanced diagnostic equipment is thus limited. In particular, direct observation and measurements on the arcs by conventional diagnostic methods are practically impossible. One has to rely on measuring integral quantities as RMS values and Fourier spectra (100, 150, 200, 250 Hz, ...) of the electrode currents and electrode-to-bottom voltages, electric power, crater pressures and electrode positions.

Numerical modelling of the electric arc contributes to improve process understanding and represents a valuable tool for optimising furnace operation and design.

Two types of AC arc models have been developed: the *Magneto-Fluid-Dynamic (MFD)* model which will be described in detail in this paper, and the *Channel Arc Model (CAM),* which was published at INFACON-8 [1].

In short, the CAM treats the arc as a cylindrical conductor with radius $R_k(t)$ and a prescribed radial temperature profile with a mean value $T_k(t)$. It is further assumed that Steenbeck's minimum energy principle is applicable in the DC case, and that an AC arc will always strive towards the equilibrium state of a DC arc with current equal to the instantaneous AC current. The CAM is coupled to a three-phase *Electric Circuit Model* [1].

The relatively simple CAM offers a quick and easy tool for predicting the electrical characteristics of the arc as a non-linear element in the electric circuit of a furnace. A detailed description of the Channel Arc Model is given elsewhere [2].

2. MAGNETO-FLUID-DYNAMIC ARC SIMULATION MODEL

2.1. Assumptions and boundary conditions

In the *Magneto-Fluid-Dynamic* (*MFD*) model time-dependent conservation equations for mass, radial and axial momentum and energy are solved together with a transport equation for the azimuthal magnetic field. The current density is then obtained from the magnetic field by Ampere's law. The output from the MFD model are the *2D* distributions of temperature $T(r,z,t)$, radial and axial velocity $v_r(r,z,t)$ and $v_z(r,z,t)$, pressure $p(r,z,t)$, magnetic flux density $B_\theta(r,z,t)$, radial and axial electric current density $j_r(r,z,t)$ and $j_z(r,z,t)$, total arc current $i(t)$ and arc voltage $u_{arc}(t)$ calculated as functions of time over an AC period.

The MFD model is combined with the same Electric Circuit Model as the Channel Arc Model [1,2].

The two **main assumptions** are the usual: *Local thermodynamic equilibrium* (*LTE*) and *Cylindrical symmetry*, which here implies that the arc axis coincides with the electrode axis and that electromagnetic interactions between the three electric phases are disregarded. It is further assumed that the composition of the crater atmosphere everywhere corresponds to a given SiO:CO molecular ratio. Buoyancy is neglected. Compressibility effects, however, are accounted for.

The **computational domain** corresponds to the generally recognised shape and size of the furnace crater including the arc region. A high level of resolution is required with a grid size as small as 0.5 mm and minimum 1,000 time-steps per AC period. This model therefore demands high computer capacity and several hours of CPU time for simulating 3 - 4 AC periods until a steady periodic solution is obtained.

2.2. Governing equations

In the MFD AC arc simulation model the following 2D conservation equations for time-varying compressible flows are used:

Conservation of **mass**:

$$\frac{\partial \rho}{\partial t} + \frac{1}{r}\frac{\partial}{\partial r}(r\rho v_r) + \frac{\partial}{\partial z}(\rho v_z) = 0$$

Conservation of **radial momentum**:

$$\frac{\partial}{\partial t}(\rho v_r) + \frac{1}{r}\frac{\partial}{\partial r}(r\rho v_r v_r) + \frac{\partial}{\partial z}(\rho v_z v_r) =$$
$$= -\frac{\partial p}{\partial r} + \frac{1}{r}\frac{\partial}{\partial r}\left(2r\mu_{eff}\frac{\partial v_r}{\partial r}\right) - \frac{\partial}{\partial r}\left(\frac{2}{3}\mu_{eff}\nabla\cdot\vec{v}\right)$$
$$+ \frac{\partial}{\partial z}\left(\mu_{eff}\left(\frac{\partial v_r}{\partial z} + \frac{\partial v_z}{\partial r}\right)\right) - \frac{2\mu_{eff}v_r}{r^2} - j_z B_\theta$$

Conservation of **axial momentum**:

$$\frac{\partial}{\partial t}(\rho v_z) + \frac{1}{r}\frac{\partial}{\partial r}(r\rho v_r v_z) + \frac{\partial}{\partial z}(\rho v_z v_z) =$$
$$= -\frac{\partial p}{\partial z} + \frac{1}{r}\frac{\partial}{\partial r}\left(r\mu_{eff}\left(\frac{\partial v_r}{\partial z} + \frac{\partial v_z}{\partial r}\right)\right)$$
$$+ \frac{\partial}{\partial z}\left(2\mu_{eff}\frac{\partial v_z}{\partial z} - \frac{2}{3}\mu_{eff}\nabla\cdot\vec{v}\right) + j_r B\theta$$

μ_{eff} is the effective *turbulent* viscosity calculated by the *k-ϵ turbulence model.*

Conservation of **energy**:

$$\frac{\partial}{\partial t}(\rho h) + \frac{1}{r}\frac{\partial}{\partial r}(r\rho v_r h) + \frac{\partial}{\partial z}(\rho v_z h) =$$
$$= \frac{\partial}{\partial r}\left(rk_{eff}\frac{\partial T}{\partial r}\right) + \frac{\partial}{\partial z}\left(k_{eff}\frac{\partial T}{\partial z}\right) + \frac{j_r{}^2 + j_z{}^2}{\sigma}$$
$$+ \frac{5k_B}{2e}\left(j_r\frac{\partial T}{\partial r} + j_z\frac{\partial T}{\partial z}\right) - S_{rad} + \frac{Dp}{Dt}$$

S_{rad} is the ***net volumetric radiation density*** [W/m^3] – see Sect. 2.6. k_{eff} is the effective *turbulent* thermal conductivity. The last term *Dp/Dt* has to be included when *compressibility* effects are significant. In addition, pressure dependent density ρ, specific enthalpy h, transport coefficients and radiation term S_{rad} should be used.

Magnetic transport equation:

$$\frac{\partial B_\theta}{\partial t} + \frac{1}{r}\frac{\partial}{\partial r}(rv_r B_\theta) + \frac{\partial}{\partial z}(v_z B_\theta) =$$
$$= \frac{\partial}{\partial r}\left(\frac{\Gamma_m}{r}\frac{\partial}{\partial r}(rB_\theta)\right) + \frac{\partial}{\partial z}\left(\Gamma_m\frac{\partial B_\theta}{\partial z}\right)$$

$\Gamma_m = 1 / \mu_0 \sigma$ is *the magnetic diffusivity*, which governs the diffusion of the AC magnetic field through the arc plasma. The time-dependent radial and axial current densities are calculated by taking the derivative of $B\theta$ according to **Ampere's law.**

2.3. Boundary conditions

Standard steady state boundary conditions for temperature (or specific enthalpy) and radial and axial velocity apply at the solid crater walls, the electrode surface and at the metal containing crater bottom with the possible exception of the cathodic arc attachment spot. The boundary conditions for the magnetic field are quite simply determined from the *time-varying arc current i(t)* by integrating Ampere's law. *i(t)* is calculated timestep by timestep using the Electric Circuit Model - see Sect. 3 [1,2].

The boundary conditions at the cathode end of the arc require special attention. In earlier versions of the MFD model a constant current density profile $j_c(r)$ is specified for the cathode spot. In the more recent version, a special Cathode Sub-Model is used together with the arc model in an iterative procedure – see Sect. 5. The cathodic current density profile $j_c(r,t)$ and the cathode fall voltage $u_c(t)$ are calculated as time-dependent quantities. In AC arcs, of course, the cathode alternates between the electrode and the metal containing crater bottom. By integrating Ampere's law the current density profiles are transformed into magnetic field distributions $B_c(r,t)$, which are then used as boundary conditions at the cathode spots.

2.4. Composition of Si-O-C plasmas

The plasma composition is required for the evaluation of thermodynamic properties and transport coefficients including radiation heat transfer data. In the industrial *silicon metal* process the main atomic components are *Si*, *O* and *C*. The crater plasma also contains small quantities of easily ionised *Al* and *Ca* vapour, which originate from contamination present in the raw materials. This implies that one must consider **the five-component system Si-O-C-Al-Ca.**

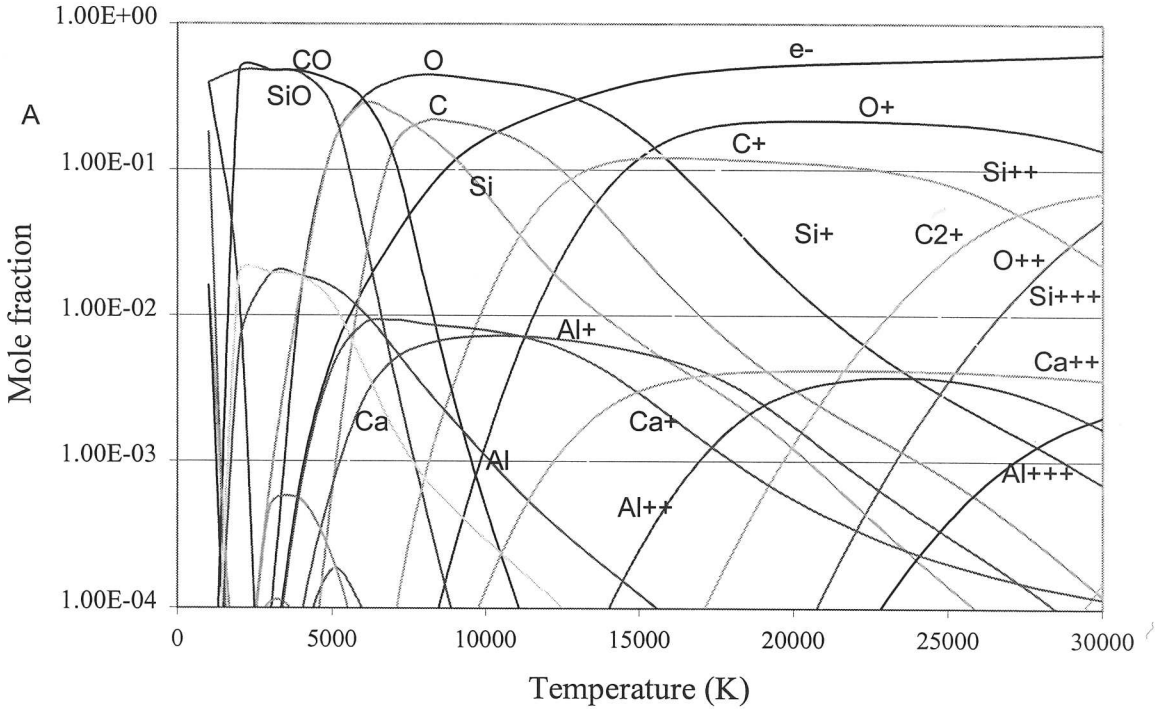

Figure 1. Composition as a function of temperature for SiO:CO = 1:1 with 1 at% Al and 1 at% Ca.

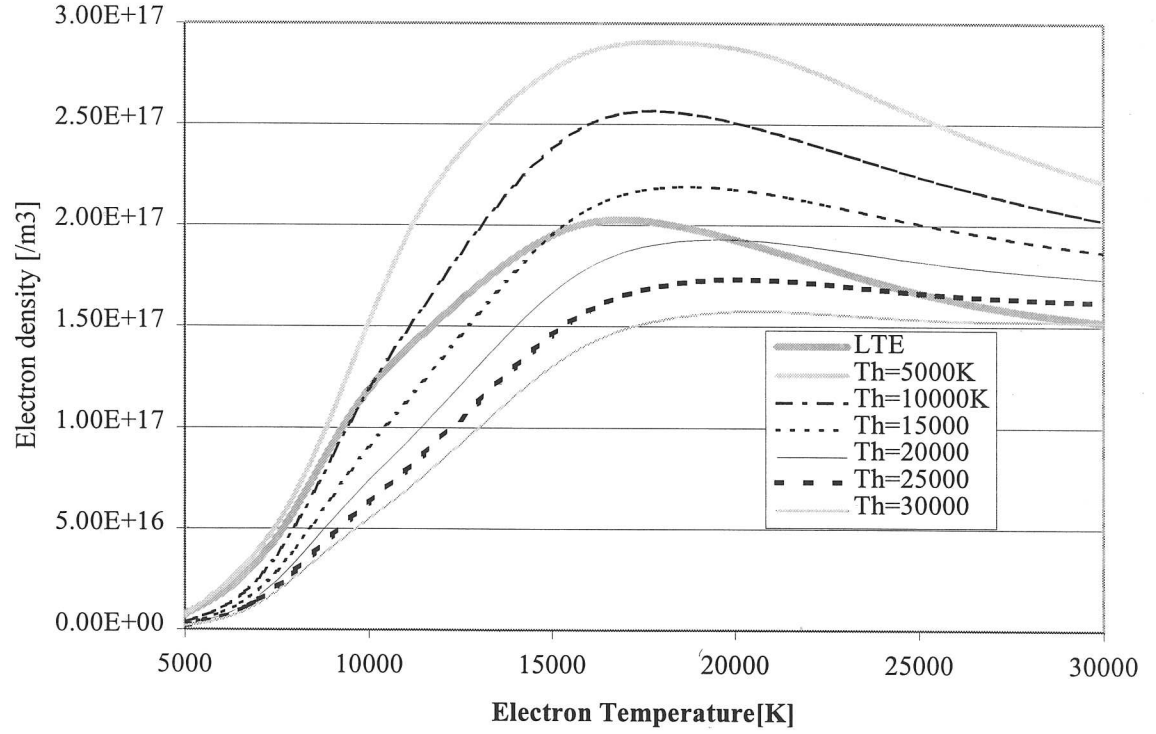

Figure 2. Electron density for a non-LTE plasma with composition SiO:CO = 1:1 The figure shows electron density as a function of electron temperature for various heavy particle temperatures T_h. The equilibrium (LTE) electron density is shown for comparison.

A specially developed computer code calculates the LTE composition in the temperature range 5,000 - 30,000 K at pressures from 0.1 to 10 bar. High-pressure data are required in order to take compressibility effects into account. For any given *atomic ratio* **Si:O:C:Al:Ca** the number densities of the following species are calculated: Electrons, Si, Si+,Si++, Si+++, Si2, O, O+, O++, O+++, O-, O2, O2+, O2-, C, C+, C++, C+++, C-, C2, C3, C2+, C2-, Al, Al+, Al++, Al+++, Ca, Ca+, Ca++, Ca+++, CO, CO+, CO2, SiO, SiO2, SiC, SiC2, Si2C, AlO, AlO+, CaO.

Figure 1 shows the composition of a plasma with atomic ratio Si:O:C:Al:Ca = 0.245 : 0.490 : 0.245 : 0.010 : 0.010 (i.e. SiO:CO = 1:1 contaminated with 1 at% Al + 1 at% Ca). It is seen that Ca+ ions are more abundant than Si+ ions below 6,500 K. In Sect. 6 it will be shown that the overall effect of Al and Ca vapour on the arc behaviour is surprisingly small.

Deviations from the LTE approximation presupposed in the arc simulations reported here, are probably present in the outer parts of the arc, and perhaps everywhere around current zero. This implies that the electrons may have a substantially higher temperature than the heavy particles, i.e. the atoms and ions This will increase the conductivity in the colder regions as the electric conductivity is mainly determined by the electron temperature – in particular close to the electrode and the crater bottom. Work has therefore been initiated to investigate the effects of non-LTE phenomena on AC arc characteristics. As an introduction, the composition of Si-O-C-Al-Ca plasmas with different electron T_e and heavy particle temperatures T_h has been calculated by means of a newly developed programme. Figure 2 shows the electron density for a non-LTE Si-O-C plasma as a function of the electron temperature for various heavy particle temperatures.

2.5. Radiation heat transfer

In submerged-arc furnaces a main part of the heat exchange within the high-current arcs and between the arcs and the charge materials is by radiation. To solve the energy equation it is necessary to calculate the *net volumetric radiation density* S_{rad} in any point of space taking into account the highly non-uniform temperature distribution in the arc. At high current levels the effect of pressure variations are also significant.

The radiation from an arc is not optically thin at all wavelengths. Some of the wavelengths will be absorbed within the radiating volume. Due to reabsorbtion, the net radiation emitted from any volume element in the arc will, in principle, depend on the temperature and pressure distribution in the rest of the arc. An exact calculation of radiation would demand enormous computer capacity. In order to decouple the calculation of S_{rad} from the calculation of the temperature field, it is desirable to account for reabsorbtion of radiation by an approximate method.

Two approaches are used in the MFD arc models: The *Integral Method of Partial Characteristics* [3] and the method of the *Effective Radiation Radius* of an isothermal sphere. A special program has been developed for calculation of optical spectra - i.e. the spectral absorbtion coefficients k_ν' - and *radiation transfer data* in plasma mixtures consisting of Si, O, C, Al and Ca [3]. In the optical spectrum, all the important radiative processes, which determine the continuum and quasi-continuum spectrum, and several hundreds of spectral lines and tens of photo-ionisation continua and molecular bands were considered.

As an example, the *net volumetric radiation density* S_{rad} is shown in Figure 3 as a function of temperature for SiO:CO = 1:1 plasmas contaminated with 1 at% Al and/or Ca vapour. The total pressure is 1 bar.

2.6. Thermodynamic properties and transport coefficients

Based on the calculated composition a computer code has been developed for calculation of all relevant thermodynamic properties and transport coefficients as functions of the atomic ratio Si:O:C:Al:Ca of the 5-component plasma mixture, the plasma temperature and the total pressure: *mass density, specific heat, specific enthalpy, electric conductivity, viscosity* and *thermal conductivity*. As an example, Figure 4 shows the *electric conductivity* for SiO:CO = 1:1 plasmas contaminated with 1 at% Al and/or Ca vapour.

In the industrial process for production of *ferrosilicon* (e.g. FeSi75 with 75 % Si) *iron* vapour will be present in the crater. The programs for calculation of plasma composition and properties are now being extended to include ***Fe*** as the 6th component.

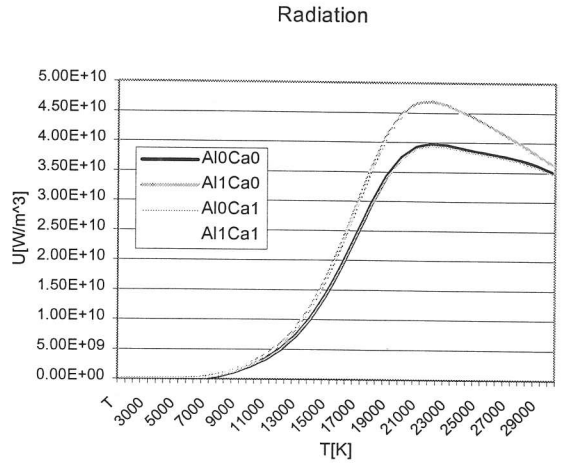

Figure 3. Net volumetric radiation density vs temperature of Si-O-C plasmas contaminated with 1 at % Al and/or 1 at% Ca.

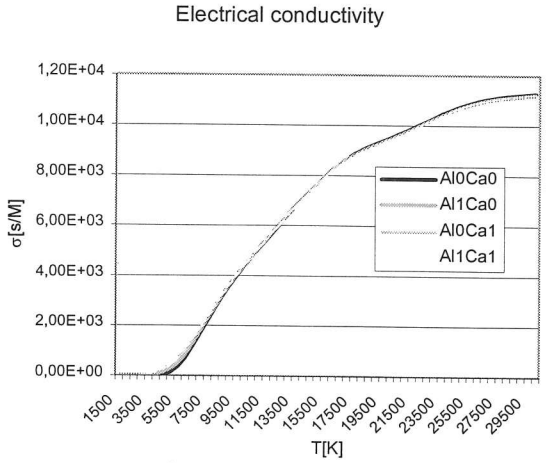

Figure 4. Electrical conductivity vs temperature of Si-O-C plasmas contaminated with 1 at% Al and/or 1 at% Ca.

3. ELECTRIC CIRCUIT DESCRIPTION

The coupling between the arcs and the AC power source as described by the *Electric Circuit Model* is crucially important for the operation of the arcs. The circuit model should take into account the complete three-phase AC circuit with transformers, self-inductances and phase-to-phase mutual inductances, rather than rely on a simplified one-phase description. This is necessary in order to predict correctly the 3N current harmonics and electrical interactions between the three phases. Further details on the circuit model have previously been reported at this conference [1].

Measurements on a ferrosilicon furnace during a melt-down period has confirmed the common view among furnace operators that typically 15-30 % of the electrode current goes through the charge and thus bypasses the arc. This is represented by an equivalent *charge resistance* R_{ch} in the electric circuit model. It was further confirmed that the arc current passes through a *series resistance* R_s, which is also introduced in the general circuit model. These conclusions are based on the generally accepted assumption that higher harmonics in the arc voltage are generated exclusively by the arc itself. Later measurements indicate that the charge does not behave linearly and therefore can produce harmonics in the voltage. This can reduce the credibility of the values for R_{ch} and R_s evaluated from the experiment, and therefore also the estimated fraction of current passing through the charge. There are also some indications for that the arc can burn from the side of the electrode, not only from the bottom. This can be the case when there is excessive electrode movement, with the electrode rising fast followed by a slower lowering of the electrode.

4. MODELLING RESULTS

4.1. Laboratory arcs

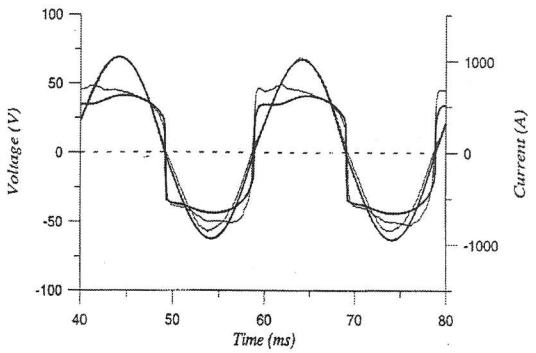

Figure 5. Simulated (thick lines) and measured (thin lines) current (almost "sinusoidal") and arc voltage waveforms for a laboratory arc in Argon, arc length 4 cm, current 650 A RMS.

In order to verify the MFD AC arc model (and also the Channel Arc Model), H.L. Larsen [4] performed extensive electrical measurements on AC arcs in a laboratory single-phase plasma reactor. Current and arc voltage waveforms, RMS values and Fourier spectra were determined for 4 cm long Argon arcs in the current range 600–1200 A. The cylindrically symmetric computational domain corresponds to the geometry of the plasma reactor and the electrodes used. The agreement between simulated and measured waveforms was quite satisfactory as can be seen from Figure 5. An interesting point is that the

MFD simulation model predicts a small DC component, which is confirmed experimentally.

4.2. Industrial arcs

MFD (as well as CAM) simulations have been performed on the high-current AC arcs expected to exist in the craters of a 30 MVA three-phase submerged-arc furnaces for production of *silicon metal*. The crater gas was supposed to consist of SiO and CO in molecular ratio 1:1 with or without Al and Ca vapour.

The computational domain again corresponds to the assumed shape and size of the crater cavity of the industrial furnace. The arc length was varied from 5 to 20 cm. It was soon found that that arc lengths of 5–10 cm gave the best fit to industrial data. The available transformer voltage is far from high enough to sustain e.g.a 20 cm long arc.

As an example, Figure 6 shows the current and voltage waveforms for a 5 cm long arc in pure SiO-CO. The voltage waveform resembles a square wave. As expected, the circuit reactance causes a phase shift between the transformer secondary voltage and the arc current. The calculated RMS current is 59 kA, which is considerably lower than the measured value 75 kA. The difference can, however, be partly explained as the charge current bypassing the arc, or that there might be two or more arcs burning in parallel, as discussed later in this paper.

The main input parameters in the Electric Circuit Model are: secondary phase voltage 128 V RMS, phase inductance 3.8 μH and phase loss resistance 0.1 mΩ.

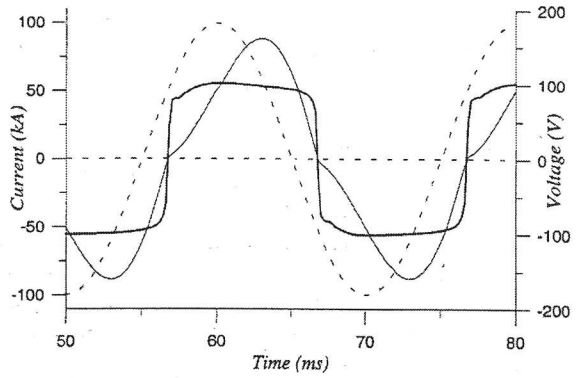

Figure 6. Simulated current and arc voltage (thick line) waveforms for arcs in a silicon metal furnace with pure SiO-CO plasma. The transformer phase voltage is shown as a broken line.

5. CATHODE SUB-MODEL FOR AC ARCS

The *AC Cathode Sub-Model* described here is based on Neumann's theory [5] and on Benilov's works [6, 7] on low-current DC arc cathodes. The cathode sub-model uses Richardson-Dushman's equation which gives *the electron emission current* j_e^{em} as a function of the cathode surface temperature and the work function ϕ: $j_e^{em} = A\,T_c^2\,exp(-e\phi/k_BT)$. Theoretically $A = 1.2{\cdot}10^6$ A/m$^2{\cdot}$K^2. The emitted electrons, which are accelerated as they pass through *the cathode voltage fall* u_c, gain sufficient energy to ionise neutral atoms from the arc column generating an *ion current* j_i. The ions accelerate towards the cathode surface, where they give off their excess energy $j_i\,(u_c + U_i - \varphi)$ thus heating up the cathode spot to the thermionic emission temperature. U_i is the ionisation potential of the gas mixture (e.g. SiO + CO). A modified version of Neumann's electron energy balance relates the electron emission current to the ion current and *the current of counter-diffusing electrons*, j_e^{mot}, from the arc plasma to the cathode. *The net heat flux* conducted into the cathode body is given roughly by

$$\dot{q}_C = j_i(u_C + U_i - \phi) - j_e{}^{em}\phi + j_e{}^{mot}\phi$$

The important time-dependent quantities to be computed by the Cathode Sub-Model are *the cathode fall voltage* $u_c(t)$ and the total *cathodic current density distribution* $j_c(r,t) = j_e^{em} + j_i - j_e^{mot}$. These are used in the arc model. In AC arcs we must consider a periodically varying cathode surface temperature, which is obtained as a solution of the transient 2D Fourier heat conduction equation for the cathode body (i.e. the electrode or crater bottom). The computational domain is assumed to be large compared to the cathode spot radius and the thermal penetration depth of 50 Hz temperature oscillations. The above expression for $\dot{q}_c\,(t)$ is used as a boundary condition.

Typical simulation results are shown in Figures 7 and 8. Here the work function ϕ = 4.75 eV and the thermal conductivity of the cathode material is 80 W/m·K. The arc length is 10 cm and Ar data are used. Figure 7 is a Lissajou figure displaying the cathode fall voltage as a function of the arc current. For comparison, corresponding characteristics for DC arc cathodes have been plotted in the same figure. It is interesting to note that for the first quarter of the AC period, the fall voltage as a function of current lies above its DC equivalent. The reason is that the electrode surface does not obtain as high a temperature under AC conditions as it would under stationary DC conditions. Only close to current

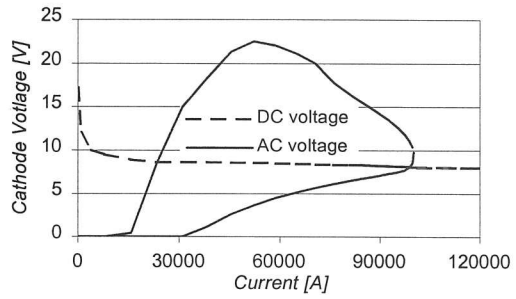

Figure 7. Cathode fall voltage $u_c(t)$ vs $i(t)$ predicted by the AC Cathode Sub-Model. Results from DC simulations are shown for comparison

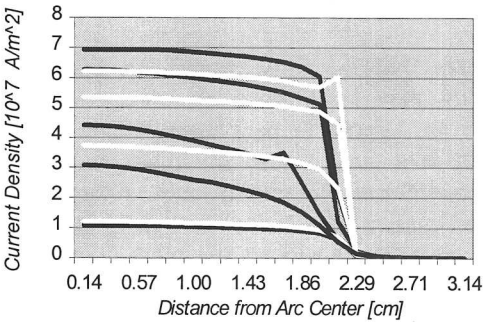

Figure 8. Predicted cathode current density $j_c(r,t)$ vs distance from the arc axis at different instants of time during the cathodic half period.

maximum does the AC fall voltage approach the DC value and thereafter it lies below. The present cathode model is inaccurate around current zero because counter-diffusing electrons have not yet been properly accounted for. As a result the total cathode current is somewhat higher than the given arc current just before and after current zero. This discrepancy is partly removed by setting the fall voltage equal to zero close to where the current shifts sign.

Figure 8 shows several curves representing the current densities at the cathode surface as a function of distance from the arc axis at various instances of time. The black lines are from the first quarter period when the arc current is rising, and the white ones are from the second quarter period where the current is decreasing.

There seems to be a clearly defined cathode spot radius, in this case 2.4 cm, which remains almost constant throughout the cathodic half-period. The current density profile also seems to be relatively uniform within that radius. This result is in conflict with the constant current density - varying spot radius assumption used previously. It also indicates that the parabolic cathode current distribution that has been implemented as an option in the arc model is less realistic than the apparently more primitive flat current profile assumption.

6. EFFECT OF EASILY IONIZED CONTAMINANTS Al AND Ca

The ionisation potentials (i.e. the energy of the first ionisation step $A \rightarrow A^+ + e^-$) of the main atomic constituents of the crater gas are: *silicon* 8.15 eV, *oxygen* 13.62 eV and *carbon* 11.26 eV. In comparison, the contaminants *aluminium* and *calcium* have considerably lower ionisation potentials: 5.99 and 6.11 eV, respectively. It was therefore expected that Al and Ca would increase the electron concentration and the electrical conductivity of the arc plasma and hence *decrease* the arc resistance. In other words, it was suspected that the presence of easily ionised pollutants in the crater gas could explain why the arc models gave consistently too high arc resistance for "reasonable" arc lengths.

A rough estimate can be made of the equilibrium partial pressures of Al and Ca vapour in the furnace crater over a typical silicon melt with 1 wt% Al and 0.15 wt% Ca at 2,000 K. The vapour pressures of the pure liquid elements are $p_{Al} = 7.5 \cdot 10^3$ Pa and $p_{Ca} = 9.5 \cdot 10^5$ Pa, respectively. The activity coefficients of Al and Ca in liquid silicon at 1,550 K are $\gamma_{Al}^{Si} = 0.38$ and $\gamma_{Ca}^{Si} = 5.2 \cdot 10^{-4}$ [8]. A rough extrapolation to 2,000 K gives $\gamma_{Al}^{Si} = 0.89$ and $\gamma_{Ca}^{Si} = 0.015$. The corresponding atom percentages of Al and Si in the gas phase at 1 bar total pressure then becomes:

1 wt% Al: $100 \cdot 0.89 \cdot 7.5 \cdot 10^3 / 1.0 \cdot 10^5 = 0.070$ at% Al
0.15wt% Ca: $100 \cdot 0.015 \cdot 9.5 \cdot 10^5 / 1.0 \cdot 10^5 = 0.014$at% Ca

The silicon melt is not in equilibrium with the slag phase. Al and Ca activities in the slag phase will be higher than for the metal phase - perhaps 2.5 times the Al concentration and 12 times the Ca concentration in the liquid metal. If the gas phase is in equilibrium with the slag phase, the gas concentrations of Al and Ca would increase proportionally, up to approximately 0.17 at% Al and 0.24 at% Ca. Also these concentrations are lower than the concentrations used in the calculations presented here: 1 at% Al and 1 at% Ca. As the metal is much more abundant than the slag, it is reasonable to assume that the gas composition is likely to be closer to equilibrium with the metal than with the slag.

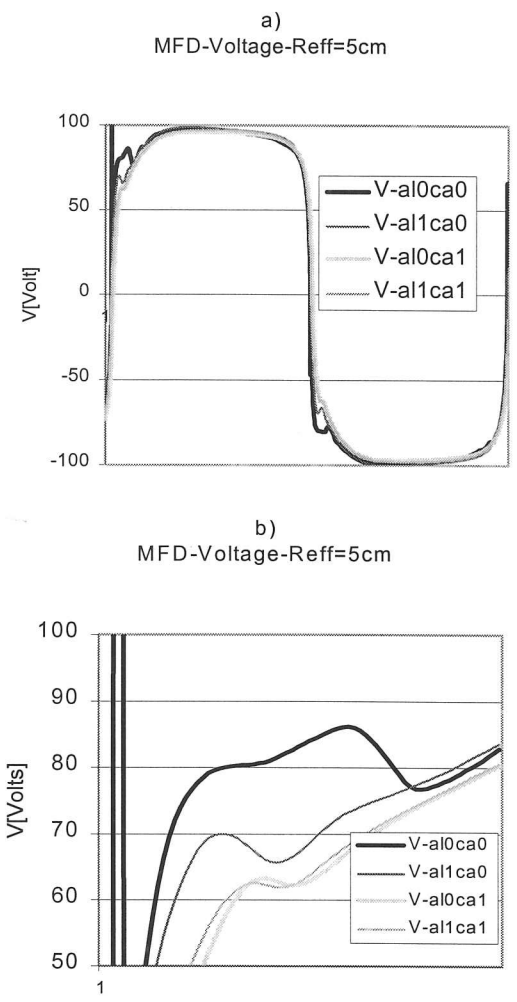

Figure 9. Comparison of voltage waveforms calculated by the MFD model for different compositions. The complete waveform is displayed in a), while b) shows in detail how the voltage rises just after passing through zero.

If a gas mixture of SiO and CO is contaminated with Al and Ca, all physical properties will be affected. The properties that have the greatest effect on arc resistance are *the electrical conductivity* σ and *the net volumetric radiation density* S_r. Radiation is important because it accounts for a great part of the energy loss from the arc. This affects the arc temperature and thereby the arc resistance.

Adding Al considerably increases the radiation, while Ca additions marginally reduce the radiation, regardless of Al content (figure 3). Therefore it is deduced that Al vapour in the plasma reduces the arc temperature, while Ca vapour has little effect.

There is no great difference in the electrical conductivity of a Si-O-C plasma depending on Al and Ca contamination at higher temperatures (Figure 4). At lower temperatures, however, there are considerable differences. Below 7,000 K there is a large difference in the electrical conductivity depending on whether the gas is contaminated or not. However, the conductivity seems to be relatively insensitive to variation in the concentration of the pollutant. 1% Al increases the conductivity less than 1% Ca does, but adding more Al does not increase the conductivity above that of a gas containing 1 at% Ca and 0 at% Al. At 4,000 K, for example, the electrical conductivity for Al1 Ca0 is more than 10 times that for pure Si-O-C, and Al1 Ca1, Al0 Ca1 and Al3 Ca1 have approximately 30 times the conductivity of pure Si-O-C gas.

This indicates that the most significant effect of contamination may be a lowering of the voltage required for an AC arc to pass through zero. That would result in a more stable arc displaying more sinusoidal waveforms for current and voltage, and this is indeed confirmed in Figure 9, which pertain to simulation results obtained with the MFD model and using the *Effective Radiation Radius* method for calculation of radiation. However, after the arc has started, the fraction of the current passing through cells with temperature below 7,000 K is negligible.

7. SPLITTING-UP OF HIGH-CURRENT AC ARCS

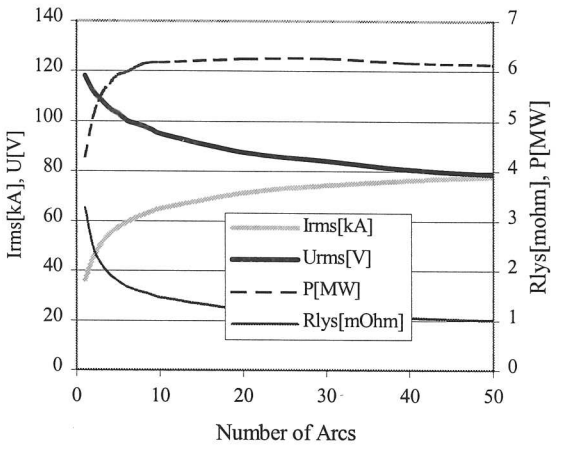

Figure 10. Electrode current and arc voltage as a function of the number of parallel sub-arcs.

CAM as well as MFD simulations with reasonable arc lengths (5 – 10 cm) give consistently higher mean arc resistance than measured in industrial furnaces. It was believed that this could be partly explained by the presence of easily ionised contaminants as Al and Ca. Another possible explanation is *arc splitting*.

According to Kaufmann's stability criterion for DC electrical arcs, several parallel arcs of equal currents can coexist stably provided that the static current-voltage characteristic is *rising*. This will lead to a lowering of the arc voltage and an increase of the current for the same transformer setting. From CAM simulations it is concluded that splitting-up of the arc in several sub-arcs will *lower* the arc voltage at a given electrode current, and thus decrease the mean arc resistance. Figure 10 shows CAM simulated electrode current and arc voltage for 5 cm long arcs in a crater gas with SiO:CO = 1:1. The phase resistance is decreased with an increasing number of sub-arcs. Note that the power released in the crater has a maximum for about 25 arcs, which gives a phase resistance of 1.19 mΩ. This is consistent with the maximum of the power vs resistance curve for the modelled furnace. These simulations assumed identical arcs, but arcs of different lengths and character could easily coexist assuming that the arc currents adjust themselves to give equal arc voltages
Due to the fact that the craters of industrial submerged-arc furnaces are inaccessible for direct visual observation of the arcs, there is no experimental evidence to neither support nor disprove the idea of multiple arc formation.

8. CONCLUSION AND SUGGESTIONS FOR FURTHER WORK

A Fluent based MHD simulation model has been developed for high current AC arcs in submerged-arc furnaces for silicon metal and ferrosilicon.

Reabsorbtion of radiation, compressibility effects (pressure dependent plasma properties) and electromagnetic induction effects are included.

A "first generation" Cathode Sub-Model for AC arcs has been developed.

Composition, thermodynamic data, transport coefficients and radiation properties under LTE-conditions are computed for 5 component plasma mixtures *Si-O-C-Al-Ca* for T = 5,000 - 30,000K and p = 0.3-10 bar.

Fe is now being included as the 6th element. Preliminary studies of the effect of *Fe* vapour on the plasma properties suggest that modelling results obtained for silicon metal furnaces are also applicable to ferrosilicon furnaces.

MFD simulations of laboratory AC arcs agreed satisfactorily with electrical measurements.

Extensive simulations of the high-current arcs in an industrial silicon furnace show that the arc length is *less than 5-10 cm*, which is much shorter than previously assumed. This conclusion is also believed to be true for *ferrosilicon* furnaces.

Al and Ca vapour from raw materials have little effect on the arc behaviour and on the arc resistance. With the actual very low crater concentrations, the RMS arc voltage probably changes by less than 1 %.

Finally, the need for further theoretical and experimental work in this industrially important field is evident from the long list of unsolved problems including:

Is the usual assumption of *local thermodynamic equilibrium* (LTE) fulfilled in high-current AC arcs in submerged-arc furnaces (and for that matter in EAFs for steelmaking)? Do deviations from LTE influence the AC arc characteristics?

A sub-model is needed for *the anode boundary layer* in high-current AC arcs.

The *depression* of the metal pool surface caused by the impinging arc should be examined.

Arc motion and instabilities probably play a role in submerged-arc furnaces, but modelling of these phenomena require a full 3D description.

LIST OF SYMBOLS

Physical quantities:

B_θ	magnetic flux density [T]
Γ_m	magnetic diffusivity [m/s^2]
γ	activity coefficient
e	electronic charge = $1.602 \cdot 10^{-19}$ [C]
h	specific enthalpy [J/kg]
i	electric current [A]
j	electric current density [A/m^2]
φ	thermionic work function [eV]
k_B	Boltzmann's constant = $1.381 \cdot 10^{-23}$ [J/K]
k_{eff}	thermal conductivity – effective turbulent [W/m·K]
k'_ν	spectral absorption coefficient [m^{-1}]
μ_{eff}	viscosity – effective turbulent [kg/m·s]
μ_0	permeability of vacuum = $4\pi \cdot 10^{-7}$ [H/m]

p	pressure [Pa, bar]
r	radial coordinate [m]
ρ	density [kg/m^3]
S_{rad}	net volumetric radiation density [W/m^3]
σ	electric conductivity [S/m]
T	temperature [K]
t	time [s]
u	voltage [V]
v	velocity [m/s]
z	axial coordinate [m]

Subscripts:

c	cathodic
e	electrons
h	heavy particles (atoms, ions)
i	ions
r	radial
z	axial

Abbreviations:

CAM	Channel Arc Model
LTE	Local Thermodynamic Equilibrium
MFD	Magneto-Fluid-Dynamic
RMS	Root-Mean-Square mean (effective) value

REFERENCES

[1] G.A. Sævarsdottir, H.L. Larsen, and J.A. Bakken, Modelling of AC Arcs in Three-Phase Submerged Arc Furnaces, INFACON-8, Beijing, China, Dec.9-12, 1996, Proceedings pp. 317-322.

[2] G.A. Sævarsdottir, H.L. Larsen and J.A. Bakken, Modelling of Industrial AC Arcs, J. High Temp. Material Processes, 3 (1999), pp 1-15.

[3] V.G. Sevastyanenko and J.A. Bakken, Radiative transfer in industrial thermal plasmas of complex composition, 5th European Conf. on Thermal Plasma Processes (TPP-5), St.Petersburg, July 13-16, 1998.

[4] H.L. Larsen and J.A. Bakken, Modelling of Industrial AC Arcs, Progress in Plasma Processing of Materials, edited by P. Fauchais, Begell House, 1997.

[5] W. Neumann, Pre-Electrode Processes in Experimental Investigation of Plasmatrons, editor M.F. Zhukov, Novosibirsk Nauka, 1977, pp 253-292 (in Russian).

[6] M.S. Benilov and A. Marotta, A model of the cathode region of atmospheric pressure arcs, J.Phys.D: Appl. Phys. 28 (1995),1869-1882.

[7] M.S. Benilov, The ion flux from a thermal plasma to a surface, J. Phys. D: Appl. Phys. 28 (1995), pp 286-294.

[8] A. Schei, J.K. Tuset and H. Tveit, "Chemistry of the Si-O-C system", in Production of High Silicon Alloys, Tapir forlag, N-7005 Trondheim, Norway.